Characterizing GCM Land Surface Schemes to Understand Their Responses to Climate Change

N. GEDNEY AND P. M. COX

Hadley Centre, The Met. Office, Bracknell, Berkshire, United Kingdom

H. DOUVILLE

Météo-France, Toulouse, France

J. POLCHER

Laboratoire de Météorologie Dynamique du CNRS, Gif-sur-Yvette, France

P. J. VALDES

Reading University, Reading, United Kingdom

(Manuscript received 8 February 1999, in final form 12 November 1999)

ABSTRACT

The impact of land surface representation on GCM simulations of climate change is analyzed using eight climate change experiments, carried out with four GCMs each utilizing two different land surface schemes (LSSs). In the regions studied (Amazonia, the Sahel, and southern Europe) the simulations differ markedly in terms of their predicted changes in evapotranspiration and soil moisture. These differences are only partly as a result of differences in the predicted changes in precipitation and available energy. A simple ''bucket model'' characterization of each LSS demonstrates that the different hydrological sensitivities are also strongly dependent on properties of the LSS, most notably the runoff, which occurs when evaporation is marginally soil moisture limited. This parameter, ''Y_c,'' varies significantly among the LSSs, and influences both the soil moisture in the $1 \times CO_2$ control climate, and the sensitivity of both evaporation and soil moisture to climate change. It is concluded that uncertainty in the predicted changes in surface hydrology is more dependent on such gross features of the runoff versus soil moisture curve than on the detailed treatment of evapotranspiration.

1. Introduction

Land surface modeling is cited as one of the major causes of the uncertainties in current climate change predictions (Houghton et al. 1996). This is especially significant given the need to assess many of the impacts of climatic change, such as the effect on agriculture and changes in the occurrence of extreme hydrological events such as drought and flooding.

Some climate simulations suggest that there will be an increased likelihood of summer drought in midlatitudes in an enhanced greenhouse gas climate (Gregory et al. 1997). Successful assessment of its potential severity is dependent on adequate modeling of the land surface. However PILPS (Henderson-Sellers et al. 1996) demonstrates that there is a wide disparity between GCM land surface schemes (LSSs), with little agreement on the modeled soil moisture and evaporation.

Koster and Milly (1997) analyzed part of the PILPS 2a experiment where identical atmospheric conditions were used to force a number of LSSs offline, which in principle have identically prescribed vegetation and soil characteristics. They showed that the hydrological behavior of the LSSs is fundamentally dependent on the interplay between evaporation and runoff, and that it was possible to understand the differences in terms of a few simple effective characteristics that can be associated with the monthly mean water balance of each LSS.

We use a similar methodology to assess the role of LSSs in predicted changes in surface hydrology as a result of climate change. This is carried out with a number of experiments using different GCMs and LSSs (described in section 2). First, the behavior of each LSS is characterized in the $1 \times CO_2$ simulations over three

Corresponding author address: Dr. N. Gedney, Hadley Centre, The Met. Office, London Rd., Bracknell, Berkshire RG12 2SY, United Kingdom.
E-mail: ngedney@meto.gov.uk

TABLE 1. LSSs used in the time-slice experiments.

Group	Notation	Description
CNRM	Ca	ISBA scheme (Noilhan and Planton 1989)
	Cb	+Reduced stomatal conductance Douville et al. (2000)
HC	Ha	Old land surface scheme (Warrilow and Buckley 1989)
	Hb	MOSES (Cox et al. 1999)
LMD	La	SECHIBA scheme (Ducoudre et al. 1993)
	Lb	Simple bucket (Manabe 1969)
UR	Ua	ECMWF scheme (Viterbo and Beljaars 1995)
	Ub	+Half the root depth

TABLE 2. The regions highlighted in this paper.

Location	Region
Amazonia	15.1°S–0.1°N and 70.1°–49.9°W
Sahel	9.9°–18.1°N and 15.1°W–25.1°E
Southern Europe	34.9°–47.0°N and 10.1°W–25.1°E

specific regions: Amazonia, the Sahel, and southern Europe (section 3a). This is achieved by examining the sensitivity of the partitioning between runoff and evapotranspiration to soil moisture for each LSS. We show that this can be used to understand the regionally averaged annual mean soil moisture of each LSS in the 1 $\times$ CO_2 control runs (section 3a).

This characterization can then be used to estimate and explain the LSS response to the change in climate forcing, as defined by changes in precipitation and available energy. The methodology for this is described in section 3b and is applied to Amazonia, the Sahel, and southern Europe in section 4.

2. Experiment

Four groups participated in the GCM experiments: the Hadley Centre (HC), the Laboratoire de Météorologie Dynamique du CNRS (LMD), Météo-France (CNRM), and the University of Reading (UR). Each performed two time-slice experiments, both consisting of a 1 $\times$ CO_2 and 2 $\times$ CO_2 run. The Atmospheric Model Intercomparison Project (AMIP; Gates 1992) sea surface temperature and sea-ice fields were used in the 1 $\times$ CO_2 experiment. The temperature and sea-ice changes produced by the Hadley Centre transient climate change run (Mitchell et al. 1995) were applied to the AMIP climatological fields to produce the boundary conditions for the 2 $\times$ CO_2 time-slice simulations. All simulations were at least 10 yr long after an initial spinup period.

Each experiment pair was implemented with two different LSSs coupled to an otherwise identical GCM. The differences between each LSS pair were not controlled, but they turned out to be mainly associated with surface hydrology (see Table 1 for a brief description of the models and the shorthand notation for each simulation). Two of the groups (HC and CNRM) included the effects of CO_2-induced stomatal closure in one of their 2 $\times$ CO_2 runs, with the 2 $\times$ CO_2 Cb simulation using the stomatal conductance changes diagnosed from Hb (Douville et al. 2000). Indeed, this was the only difference between Ca and Cb, so these models share the same 1 $\times$ CO_2 control run.

Although most of the LSSs share similar underlying assumptions, there are some LSS specific points that are worth noting. First, the bucket model used in ''Lb'' may be considered as slightly anomalous since this is the very simplest LSS used in early GCM simulations (Manabe 1969). It is included here because it represents one end of the range of LSS complexity, and also because it is still in use in some climate and numerical weather prediction models. Offline intercomparisons have suggested that the behavior of the bucket model differs from more complex LSSs primarily because it does not include an additional surface resistance to evaporation (Henderson-Sellers et al. 1996). However, the bucket model also relies on a different runoff generation mechanism than most current day LSSs, which are often dominated by slow ''Darcian'' drainage. By contrast, the bucket produces runoff only when the soil moisture exceeds the specified field capacity, which makes this model more sensitive to the temporal variability of the rainfall. Of the other LSSs used here, only SECHIBA (Schématisation des Echanges Hydriques à l'Interface entre la Biosphère et l'Atmosphère; Ducoudre et al. 1993) as used in La, is likely to share this sensitivity. Also, the novel soil moisture scheme in this model means that there is no simple relationship between rootzone soil moisture and evapotranspiration, because vegetation becomes unstressed if the movable top layer of soil becomes saturated, even if the rootzone as a whole is moisture deficient.

These LSS differences are relevant to the next section where we analyze the behavior of each model in the three distinct regions of Amazonia, the Sahel, and southern Europe. Table 2 lists the latitude and longitude ranges defining these study areas.

3. Characterizing the land surface schemes

Following the general approach of Koster and Milly (1997), a ''bucket-type'' formulation is utilized to model how the suite of LSSs respond to limited soil moisture under snow-free conditions and ignoring interception, E_i.

In the usual bucket model actual evaporation is calculated as the product of a soil moisture stress (''β'') factor and the potential evaporation rate, E_p (Manabe 1969). Unfortunately, the potential evaporation rate was not available from all of the GCM experiments, so we replaced E_p in the usual bucket formulation with effective available energy, A_e:

$$A_e = \frac{R_N - G - LE_i}{L}. \quad (1)$$

Here A_e has been scaled to have the units of a water flux, and R_N, G, and L are the net radiation, the ground heat flux, and the latent heat of vaporization. (We also define the effective available energy as $A_e = A - E_i$, where A is the available energy.) In this model, evapotranspiration (i.e., bare soil evaporation plus transpiration), E_e, is therefore assumed to be dependent on the effective available energy, A_e, and the rootzone soil moisture, M, through a soil moisture–dependent evaporative fraction, f:

$$E_e = fA_e. \quad (2)$$

This equation is very closely related to the standard bucket model as applied by Koster and Milly (1997), because potential evaporation and effective available energy, A_e, are strongly correlated. Correlation coefficients, between monthly mean values of E_p and A_e, were found to be well in excess of 0.9 for all of the GCMs that produced both of these diagnostics.

For convenience the soil moisture is scaled by its active range, which is defined as the point at which evapotranspiration starts (M_{wilt}) to the point beyond which evapotranspiration is not constrained by soil moisture (M_{crit}):

$$\mu = \frac{M - M_{\text{wilt}}}{M_{\text{crit}} - M_{\text{wilt}}}. \quad (3)$$

The critical and wilting points were estimated from the regionally averaged values of the parameters in each LSS. In terms of this scaled variable, f takes the simple piecewise linear dependence:

$$f(\mu) = \begin{cases} f_c\mu & \text{for } \mu < 1 \\ f_c & \text{for } \mu \geq 1, \end{cases} \quad (4)$$

where f_c is the evaporative fraction at the critical soil moisture concentration. Among the more complex LSSs f_c tends to vary due to differences in the parameterization of stomatal resistance.

Assuming that drainage dominates over surface runoff, the total runoff, Y, is likely to be most dependent on deep soil moisture, but for simplicity it is assumed that rootzone soil moisture provides a good surrogate variable (i.e., that changes in the soil moisture vertical profile are insignificant). Runoff is taken to vary with a power, c, of the scaled soil moisture, which is consistent with the Clapp and Hornberger (1978) curves used in many LSSs and is sufficiently general to fit the runoff from most other models:

$$Y = Y_c\mu^c. \quad (5)$$

Figures 1a and 1b show the variation of f and Y with μ, for the Amazonian region, as diagnosed using monthly means from each of the $1 \times CO_2$ simulations. There are a number of things to notice about these curves. First, there is a definite tendency for the gradient of f with respect to μ to be significant for $\mu < 1$ and small for $\mu > 1$, in general agreement with Eq. (4). Soil moisture heterogeneity across the region acts to smooth any such underlying f curve (Entekhabi and Eagleson 1989), but the piecewise linear form still appears to provide a good qualitative description. In some cases the soil moisture stress seems unrealistic [e.g., continual moisture stress in Amazonia (e.g., Ua, Ub, La, Lb) and negligible stress throughout most of the year in the Sahel (e.g., Hb)]. The second thing to note, is that the runoff curves from the various models differ markedly, with some models producing negligible runoff at the critical point (e.g., Ha, Hb) and others producing significant runoff even at much lower soil moistures (e.g., Ua, Ub, La, Lb). In general the models give runoff values that increase monotonically with soil moisture, but there is also some evidence of hysteresis in the Y–μ curve. Last, it is clear that the models tend to occupy quite distinct μ-regimes, with some models rarely experiencing moisture stress (e.g., Ha, Hb) and others remaining moisture stressed throughout the year (e.g., Ua, Ub, La, Lb). This distinction is partly a consequence of the underestimate of Amazonian precipitation in the latter models, but throughout this paper we will show that differences in the LSSs also play a major role, both in Amazonia and elsewhere.

The relatively small range of μ experienced by each LSS allows us to use a linear approximation for the stress and runoff curves:

$$f(\mu) = f_c + f'(\mu - 1), \quad (6)$$

$$Y(\mu) = Y_c + Y'(\mu - 1), \quad (7)$$

where f' and Y' are the gradients of f and Y with respect to μ, and f_c and Y_c are the values of f and Y at the critical point ($\mu = 1$).

For each model the monthly mean values of Y and E_e/A_e from the control runs were fitted to Eqs. (7) and (6), respectively, using a least squares regression. For Amazonia and the Sahel all 12 months were utilized in the fitting exercise, but for the southern European region only the months from April to September were used, to avoid periods when the available energy is so small that f is ill-defined. This procedure provides an estimate of the characteristics of each LSS in terms of f_c, Y_c, f', and Y'. Values for Amazonia, the Sahel, and southern Europe are given in Tables 3, 4, and 5.

a. Estimating the surface hydrology of the control climate

In this section we test the characterization of each LSS by attempting to predict its long-term mean soil moisture status and annual mean evaporation $\overline{E}$ using information about the $1 \times CO_2$ control climates. On the multiannual timescale, changes in soil moisture storage are negligible, so throughfall precipitation (i.e., precip-

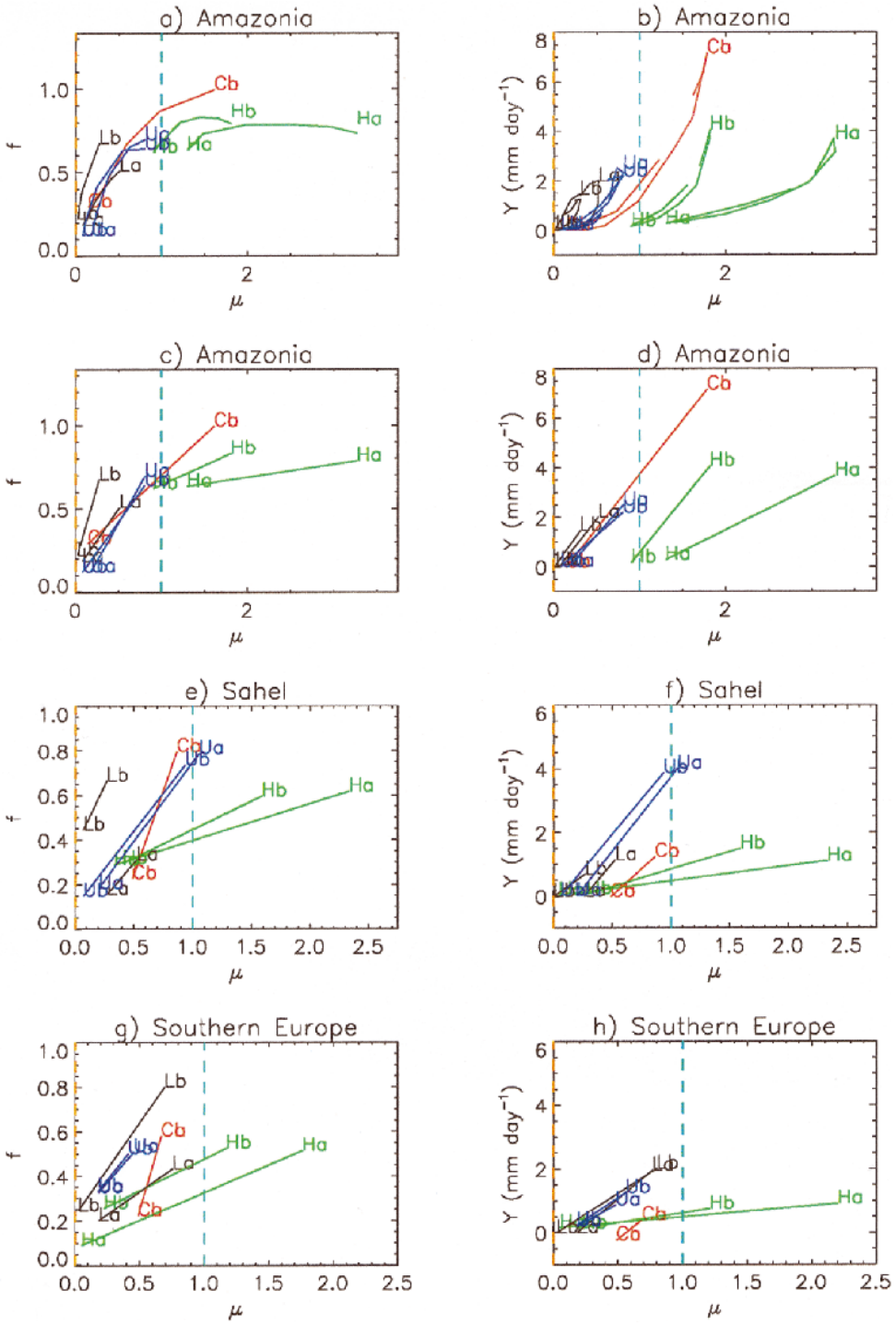

FIG. 1. The dependence of runoff and evaporative fraction on scaled soil moisture in the control climates. Plots (a) and (b) correspond to the raw monthly mean GCM data for Amazonia, while the other plots are linear model fits to Amazonia, the Sahel, and southern Europe. Each color corresponds to a different GCM (LMD—Black, CNRM—Red, Hadley Centre—Green, University of Reading—Blue).

TABLE 3. Bucket model fitting parameters (f_c, f', Y_c, Y'), aridity index (ϕ), runoff fraction at the critical soil moisture (χ), ratio of the sensitivities of evaporation and runoff to soil moisture (ζ), and estimated sensitivities of evaporation to throughfall and effective available energy ($\partial E_e/\partial P_e$ and $\partial E_e/\partial A_e$) for the Amazonian region. Values in brackets refer to the root-mean-square error.

Parameter	Ca	Cb	Ha	Hb	La	Lb	Ua	Ub
f_c	0.76	0.76	0.68	0.68	0.87	1.94	0.81	0.74
f'	0.42	0.42	0.03	0.16	0.69	1.72	0.77	0.62
	(0.08)	(0.08)	(0.04)	(0.05)	(0.04)	(0.05)	(0.08)	(0.08)
Y_c (mm day^{-1})	2.53	2.53	−0.56	0.6	2.79	4.28	2.81	2.75
Y' (mm day^{-1})	4.13	4.13	1.51	3.82	2.78	4.33	3.72	3.25
	(0.90)	(0.90)	(0.45)	(0.54)	(0.56)	(0.27)	(0.38)	(0.40)
ϕ	0.45	0.45	0.58	0.56	1.53	2.92	1.19	1.02
χ	0.56	0.56	−0.13	0.14	1.15	1.15	1.40	1.31
ζ	0.27	0.27	0.07	0.16	1.06	2.23	0.61	0.55
$\partial E_e/\partial P_e$	0.21	0.21	0.07	0.13	0.51	0.67	0.38	0.36
$\partial E_e/\partial A_e$	0.53	0.53	0.67	0.65	0.18	0.17	0.23	0.25

itation $\overline{P}$ minus interception) balances evapotranspiration and runoff:

$$\overline{E}_e + \overline{Y} = \overline{P}_e, \tag{8}$$

where the bars denote multiannual means. Substituting in Eqs. (2), (6), and (7) gives:

$$\overline{A}_e[f_c + f'(\overline{\mu} - 1)] + Y_c + Y'(\overline{\mu} - 1) = \overline{P}_e. \tag{9}$$

Thus our simple model gives an estimate of the long-term annual mean value of μ in terms of the control climate ($\overline{P}_e$ and $\overline{A}_e$) and the surface characteristics (f_c, f', Y_c, and Y'):

$$\overline{\mu} = \frac{\overline{P}_e + \overline{A}_e(f' - f_c) + Y' - Y_c}{\overline{A}_e f' + Y'}. \tag{10}$$

Substituting this form for $\overline{\mu}$ into Eqs. (2) and (6) also yields an expression for $\overline{E}_e$. Figure 2 compares the estimated values of $\overline{\mu}$ and the annual mean evaporation to the long-term means taken from each of the $1 \times CO_2$ GCM runs. [The estimates of annual mean evaporation were calculated by adding the GCM interception rates onto the expression for $\overline{E}_e$. The annual mean quantities for P_e and A_e were used for calculating μ and E in all the regions studied, even though the linear fit for southern Europe was based on data from April to September alone (see section 3).] The simple linear characterization of each LSS is clearly able to capture the large variation in moisture stress and evaporation between the models, for each of the three regions.

Insight into the reasons for the discrepancies between the models can be gained by examining the conditions required for the annual mean evaporation not to be moisture limited. From Eq. (9), $\overline{\mu} \geq 1$, if

$$\chi \leq 1 - \phi, \tag{11}$$

where we have defined two new dimensionless parameters:

$$\phi = \frac{f_c \overline{A}_e}{\overline{P}_e}, \tag{12}$$

$$\chi = \frac{Y_c}{\overline{P}_e}. \tag{13}$$

The parameter, ϕ, is akin to Budyko's aridity index as described by Koster and Suarez (1999), while χ represents the runoff fraction when $\overline{\mu} = 1$. Figure 3a plots all regional values for each model in the χ–ϕ phase space. The dot–dashed line represents $\phi + \chi = 1$, with evaporation being moisture limited in all models to the right of this line. The large variation in ϕ for a given region between the schemes indicates that the control climates differ markedly, and therefore some must be unrealistic. Moreover there is no clear ranking of ϕ

TABLE 4. Bucket model fitting parameters (f_c, f', Y_c, Y'), aridity index (ϕ), runoff fraction at the critical soil moisture (χ), ratio of the sensitivities of evaporation and runoff to soil moisture (ζ), and estimated sensitivities of evaporation to throughfall and effective available energy ($\partial E_e/\partial P_e$ and $\partial E_e/\partial A_e$) for the Sahelian region. Values in brackets refer to the root-mean-square error.

Parameter	Ca	Cb	Ha	Hb	La	Lb	Ua	Ub
f_c	0.94	0.94	0.41	0.45	0.65	2.3	0.82	0.81
f'	0.52	0.52	0.17	0.33	0.71	2.14	0.69	0.63
	(0.10)	(0.10)	(0.07)	(0.07)	(0.02)	(0.08)	(0.11)	(0.11)
Y_c (mm day^{-1})	1.15	1.15	0.38	0.55	1.99	1.87	3.19	3.32
Y' (mm day^{-1})	1.00	1.00	0.39	0.90	2.77	1.92	4.37	3.94
	(0.25)	(0.25)	(0.16)	(0.23)	(0.31)	(0.10)	(0.43)	(0.46)
ϕ	1.68	1.68	0.80	0.84	2.16	4.06	0.99	1.01
χ	0.87	0.87	0.22	0.30	1.68	0.78	1.62	1.76
ζ	1.24	1.24	1.44	1.23	1.01	5.34	0.37	0.38
$\partial E_e/\partial P_e$	0.55	0.55	0.59	0.55	0.50	0.84	0.27	0.27
$\partial E_e/\partial A_e$	0.21	0.21	0.17	0.18	0.11	0.07	0.32	0.30

TABLE 5. Bucket model fitting parameters (f_c, f', Y_c, Y'), aridity index (ϕ), runoff fraction at the critical soil moisture (χ), ratio of the sensitivities of evaporation and runoff to soil moisture (ζ), and estimated sensitivities of evaporation to throughfall and effective available energy ($\partial E_e/\partial P_e$ and $\partial E_e/\partial A_e$) for the southern European region. Values in brackets refer to the root-mean-square error.

Parameter	Ca	Cb	Ha	Hb	La	Lb	Ua	Ub
f_c	1.16	1.16	0.37	0.51	0.43	1.02	0.75	0.91
f'	0.57	0.57	0.24	0.30	0.21	0.75	0.47	0.66
	(0.04)	(0.04)	(0.05)	(0.04)	(0.07)	(0.03)	(0.04)	(0.04)
Y_c	0.97	0.97	0.42	0.54	1.96	2.39	1.81	2.00
Y' (mm day^{-1})	0.74	0.74	0.28	0.55	2.52	2.54	1.99	2.23
	(0.14)	(0.14)	(0.18)	(0.10)	(0.45)	(0.31)	(0.13)	(0.14)
ϕ	2.04	2.04	0.62	0.80	0.71	1.08	0.80	0.90
χ	1.07	1.07	0.31	0.37	0.25	0.27	0.47	0.53
ζ	1.23	1.23	1.94	1.23	0.24	1.16	0.40	0.48
$\partial E_e/\partial P_e$	0.55	0.55	0.67	0.55	0.19	0.54	0.28	0.33
$\partial E_e/\partial A_e$	0.17	0.17	0.10	0.18	0.27	0.24	0.40	0.37

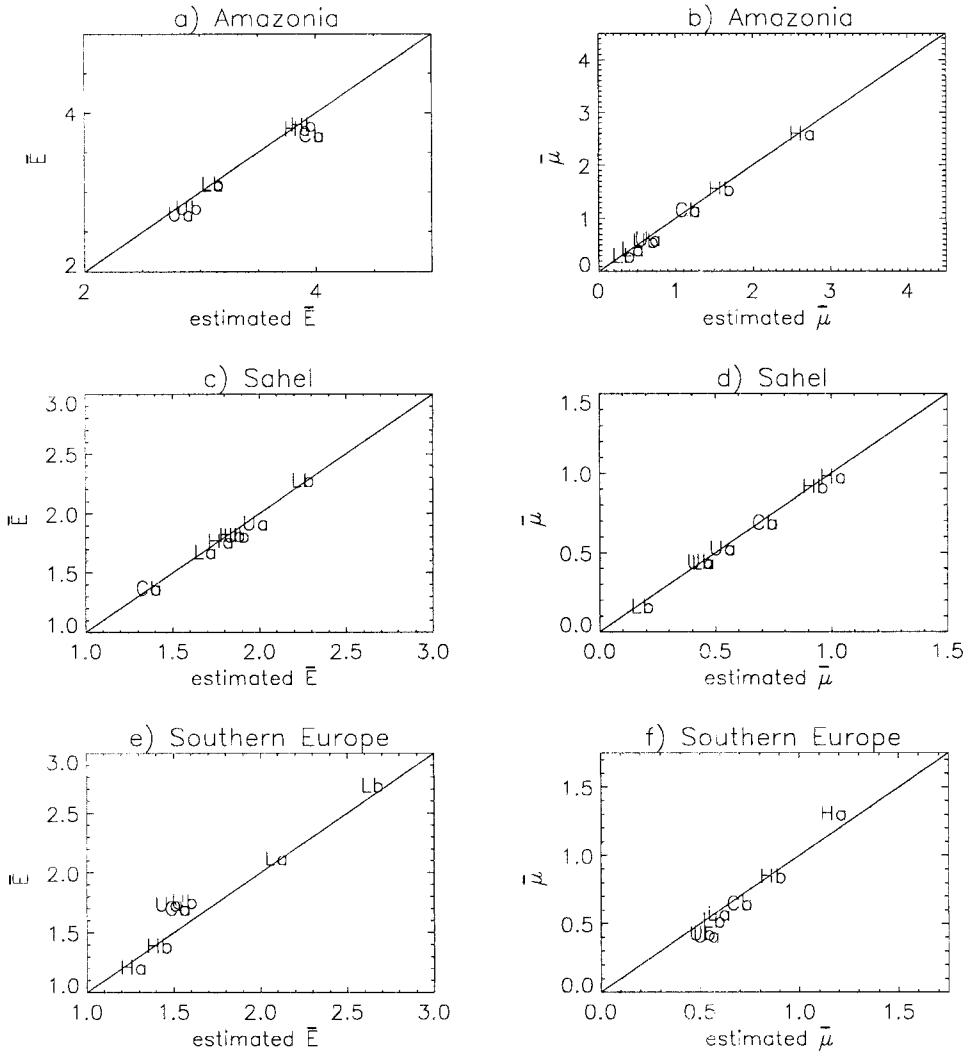

FIG. 2. GCM annual mean evaporation (E) and scaled soil moisture (μ) in the control climates vs estimates from the linear LSS characterization for Amazonia, the Sahel, and southern Europe.

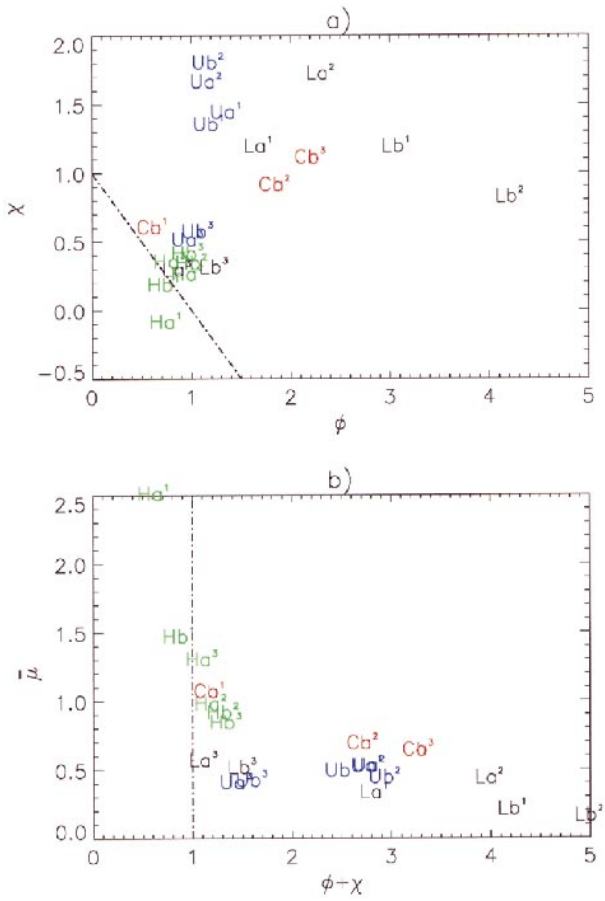

FIG. 3. Annual mean parameters from each of the model control climates and for each of the regions, with subscripts denoting the region (1—Amazonia; 2—Sahel; 3—southern Europe). (a) The positions in the χ vs ϕ phase space; (b) the mean soil moisture stress ($\overline{\mu}$) as a function of $\phi + \chi$. In both plots, models to the right of the dot–dashed line are moisture stressed.

between the regions, with, for instance, Amazonia being more arid than the Sahel in some models.

For each model there is a range of χ values that is largely associated with the different climatic regimes (as denoted by the subscripts). The values of χ also show some clustering according to LSS. Thus, for example, the Hadley Centre models (''H'') typically have small values of runoff at the critical point, which implies low values of χ, and little or no soil moisture limitation. On the other hand, the University of Reading models (''U'') always have much higher values of Y_c, usually resulting in larger χ values, ensuring that they are moisture limited in all three regions.

Figure 3b plots values of $\overline{\mu}$ against $\phi + \chi$, for each of the $1 \times CO_2$ simulations over each of the study areas. Low $\overline{\mu}$ values are associated with high values of $\phi + \chi$, which can arise from either the aridity of the driving climate (i.e., high ϕ) or from high values of runoff at the critical point (i.e., high χ).

Figure 3a shows that in many cases there is substantially more scatter in χ than ϕ. This suggests that differences in the runoff curves (Y_c) are at least as important as differences in the GCM driving climates and f_c, and in some cases Y_c is the dominant source of discrepancy among the models. This can be demonstrated further by forcing all the LSSs with the same climate for Amazonia (i.e., the same A_e and P_e). Any major differences in the resulting LSS states must then be the result of differences in the LSSs (i.e., differences in f_c and Y_c). If we take the annual mean effective available energy (3.7 mm day^{-1}) and throughfall (4.3 mm day^{-1}) from the most unstressed model, Ha (see Fig. 1a), the resulting values of $\phi + \chi$ are greater than unity for all the LSSs other than Ha and Hb (see Table 3 for values of Y_c and f_c). This indicates that only Ha and Hb would be unstressed under such a climate. With the exception of the bucket model, most of the differences between the LSSs are a result of Y_c rather than f_c, indicating that Y_c plays the largest role in the differences between the LSSs.

b. *Estimating the hydrological response to climate change*

Having demonstrated that the simple linear characterization can capture the annual mean surface hydrology predicted by each LSS, here we extend the method to analyze the changes in surface hydrology on doubling CO_2. Specifically, we consider the changes in annual mean soil moisture and evaporation arising from a prescribed climate change, as given by the changes in annual mean throughfall precipitation, $\Delta\overline{P}_e$, and effective available energy, $\Delta\overline{A}_e$. The perturbation equation for the annual mean hydrological balance [Eq. (9)] is

$$\Delta\overline{A}_e[f_c + f'(\overline{\mu} - 1)] + \Delta\overline{\mu}(\overline{A}_e f' + Y') = \Delta\overline{P}_e, \quad (14)$$

where $\Delta\overline{\mu}$ is the change in the scaled annual mean soil moisture resulting from the prescribed climate perturbation ($\Delta\overline{P}_e$ and $\Delta\overline{A}_e$). The expression for $\Delta\overline{\mu}$ can be simplified using Eq. (6):

$$\Delta\overline{\mu} = \frac{1}{Y'(1 + \zeta)}\Delta\overline{P}_e - \frac{\overline{f}}{Y'(1 + \zeta)}\Delta\overline{A}_e. \quad (15)$$

Here, a further dimensionless parameter, ζ, has been introduced, which represents the ratio of the sensitivities of evaporation and runoff to soil moisture:

$$\zeta = \frac{f'\overline{A}_e}{Y'}. \quad (16)$$

The corresponding perturbation to the evaporation is derived from Eqs. (2) and (6):

$$\Delta\overline{E}_e = \overline{f}\,\Delta\overline{A}_e + f'\overline{A}_e\Delta\overline{\mu}. \quad (17)$$

The soil moisture perturbation $\Delta\overline{\mu}$ can be eliminated using Eq. (15), to give an expression for the change in the annual mean evaporation resulting from $\Delta\overline{A}_e$ and $\Delta\overline{P}_e$:

$$\Delta\overline{E}_e = \frac{\zeta}{1+\zeta}\Delta\overline{P}_e + \frac{f}{1+\zeta}\Delta\overline{A}_e. \tag{18}$$

This equation has been written in the form of the ''chain rule'' to allow easy identification of the coefficients representing the sensitivity of evaporation to precipitation and available energy, respectively:

$$\frac{\partial\overline{E}_e}{\partial\overline{P}_e} = \frac{\zeta}{1+\zeta} \qquad \frac{\partial\overline{E}_e}{\partial\overline{A}_e} = \frac{\overline{f}}{1+\zeta}. \tag{19}$$

Values for these coefficients, as diagnosed from the 1 $\times$ CO_2 control climates, are given in Tables 3, 4, and 5. The variation among them can be understood in terms of the dependencies of $\overline{f}$ and ζ on the control state. Consider the extreme cases of a very dry soil ($\overline{\mu} \ll 1$), for which the evaporative fraction will be strongly dependent on soil moisture, and a very wet soil ($\overline{\mu} \gg 1$), for which the evaporative fraction will be independent of soil moisture:

$$f' \sim \begin{cases} f_c & \text{for } \overline{\mu} \ll 1 \\ 0 & \text{for } \overline{\mu} \gg 1, \end{cases} \tag{20}$$

where we have assumed $f(0) \sim 0$ in Eq. (6). If the Y–μ curve also passes close to the origin (such that $Y' \sim Y_c$), Eq. (20) can be substituted into Eq. (10) to give an expression for ζ in each of these two regimes:

$$\zeta \sim \begin{cases} \dfrac{\phi}{\chi} & \text{for } \overline{\mu} \ll 1 \\ 0 & \text{for } \overline{\mu} \gg 1. \end{cases} \tag{21}$$

Now substituting Eq. (21) into Eq. (19) and using $\overline{\mu}$ from Eq. (10) yields expressions for the evaporation sensitivity coefficients explicitly in terms of the control climate (through ϕ) and the LSS characteristics (through χ and f_c):

$$\frac{\partial\overline{E}_e}{\partial\overline{P}_e} \sim \begin{cases} \dfrac{\phi}{\phi+\chi} & \text{for } \overline{\mu} \ll 1 \\ 0 & \text{for } \overline{\mu} \gg 1 \end{cases} \tag{22}$$

$$\frac{\partial\overline{E}_e}{\partial\overline{A}_e} = \begin{cases} \dfrac{f_c\chi}{(\phi+\chi)^2} & \text{for } \overline{\mu} \ll 1 \\ f_c & \text{for } \overline{\mu} \gg 1. \end{cases} \tag{23}$$

Equations (11), (22), and (23) enable the LSS behavior to be summarized as follows:

- In a moist climate (i.e., where $\phi \leq 1$):
  - —An LSS may be stressed or unstressed depending on its value of χ (i.e., its runoff at the critical point, Y_c), as is illustrated by Eq. 11.
  - —In unstressed models ($\overline{\mu} \gg 1$) evapotranspiration is independent of throughfall, but optimally dependent on effective available energy.
  - —In stressed models ($\overline{\mu} \ll 1$) evapotranspiration is dependent on both the effective available energy and throughfall. These dependencies both tend to reduce with increasing χ (i.e., increasing Y_c).
- In a more arid climate (i.e., where $\phi > 1$):
  - —All LSSs are moisture limited (for physically realistic values of $\chi > 0$).
  - —The LSSs are mainly sensitive to throughfall, and this sensitivity reduces with increasing Y_c.

We use this framework to explain the regional responses as described in the next section.

4. Climate change prediction

In this section the GCM climate change predictions are analyzed for each of the three regions using the LSS characterization as a framework for understanding the model differences. Figures 4, 5, and 6 are used to summarize the findings for Amazonia, the Sahel, and southern Europe, respectively. In each case, plots a and b compare the GCM simulations of climate and surface hydrology for the control state, while c and d do likewise for the predicted climate change. Plots e and f test the ability of the characterization to reproduce the changes in evaporation and scaled soil moisture for each GCM. The ''estimated'' values were derived by applying the GCM changes in throughfall ($\Delta\overline{P}_e$) and effective available energy ($\Delta\overline{A}_e$) to Eqs. (18) and (15). The GCM changes in interception were added to the calculated value of $d\overline{E}_e$ to produce the estimated changes in total evaporation ($d\overline{E}$), as shown in the e plots. Plots g and h of each figure make use of the linear characterization to diagnose the relative sensitivities of each model to changes in throughfall and available energy. A detailed description for each region follows, and section d provides a summary of the main points.

a. Amazonia

Figure 4a shows that the control climates for Amazonia tend to be paired by GCM, with the CNRM and Hadley Centre GCMs producing much more rainfall than the LMD and University of Reading models. In this region the Hadley Centre simulations are closest to the observed annual mean precipitation (New et al. 1999). Precipitation appears to be correlated with evaporation and runoff, but there is no obvious correlation between available energy and evaporation, as might be expected in a humid climate. The climate forcing and surface response anomalies are much less paired by GCM (Fig. 4c), with each of the climate change experiments yielding qualitatively similar changes in forcing (i.e., a reduction in precipitation and an increase in available energy). Nevertheless, the hydrological responses of the LSSs differ, with two of the LSSs (Ha and Ca) producing an increase in evaporation and the other six showing a decrease (Fig. 4d).

These differences can be understood in terms of the characterization introduced in section 3, which suc-

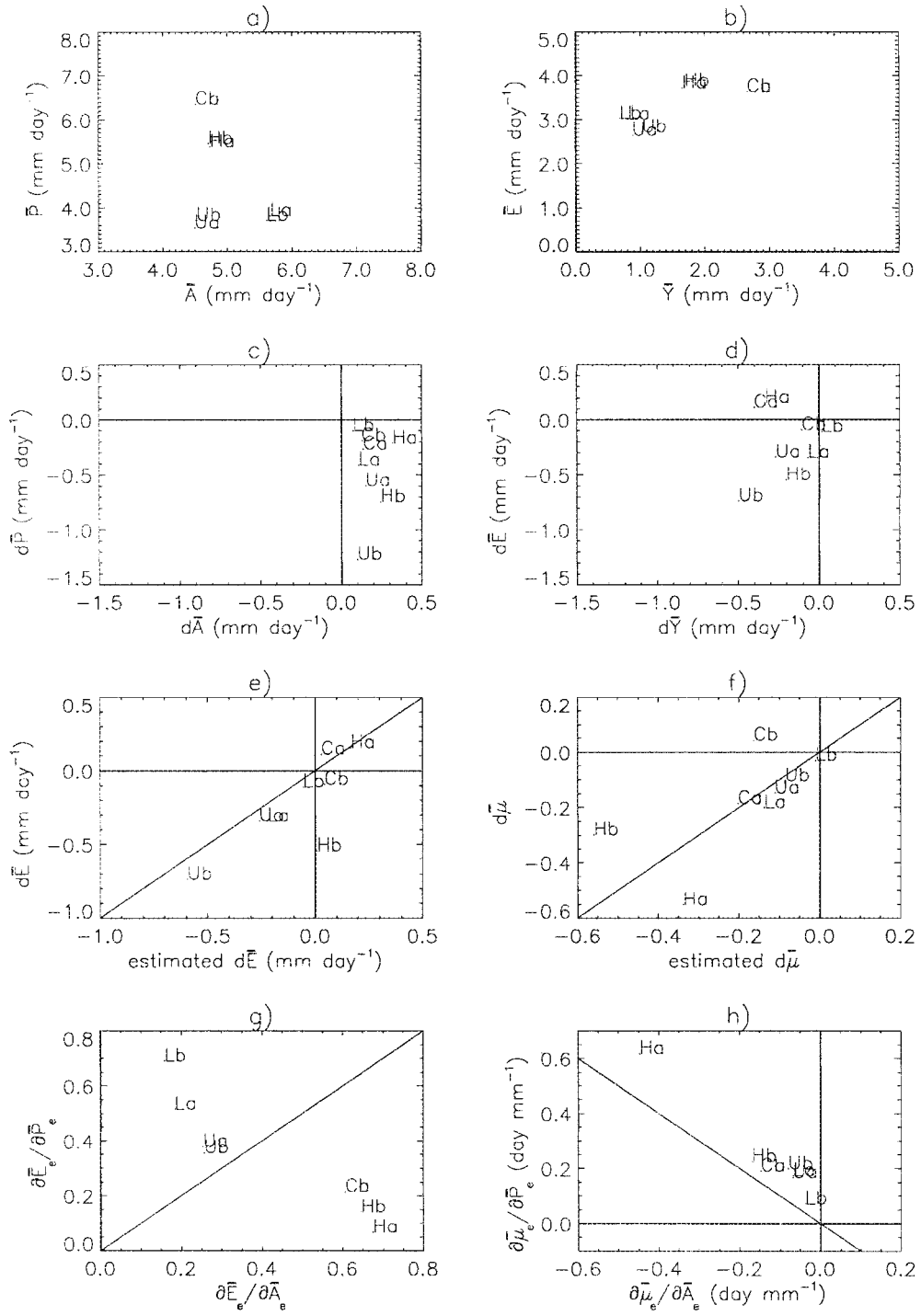

FIG. 4. GCM predictions and the linear LSS characterizations for Amazonia. (a) GCM annual mean climate; (b) GCM annual mean hydrological fluxes; (c) GCM predicted climate change; (d) GCM predicted hydrological change; (e) GCM evaporation change vs the estimate from the linear characterization; (f) GCM soil moisture change vs the estimate from the linear characterization; (g) estimated evaporation sensitivity coefficients; (h) estimated soil moisture sensitivity coefficients. [The observed annual mean precipitation from New et al. (1999) is 5.8 mm day^{-1}.]

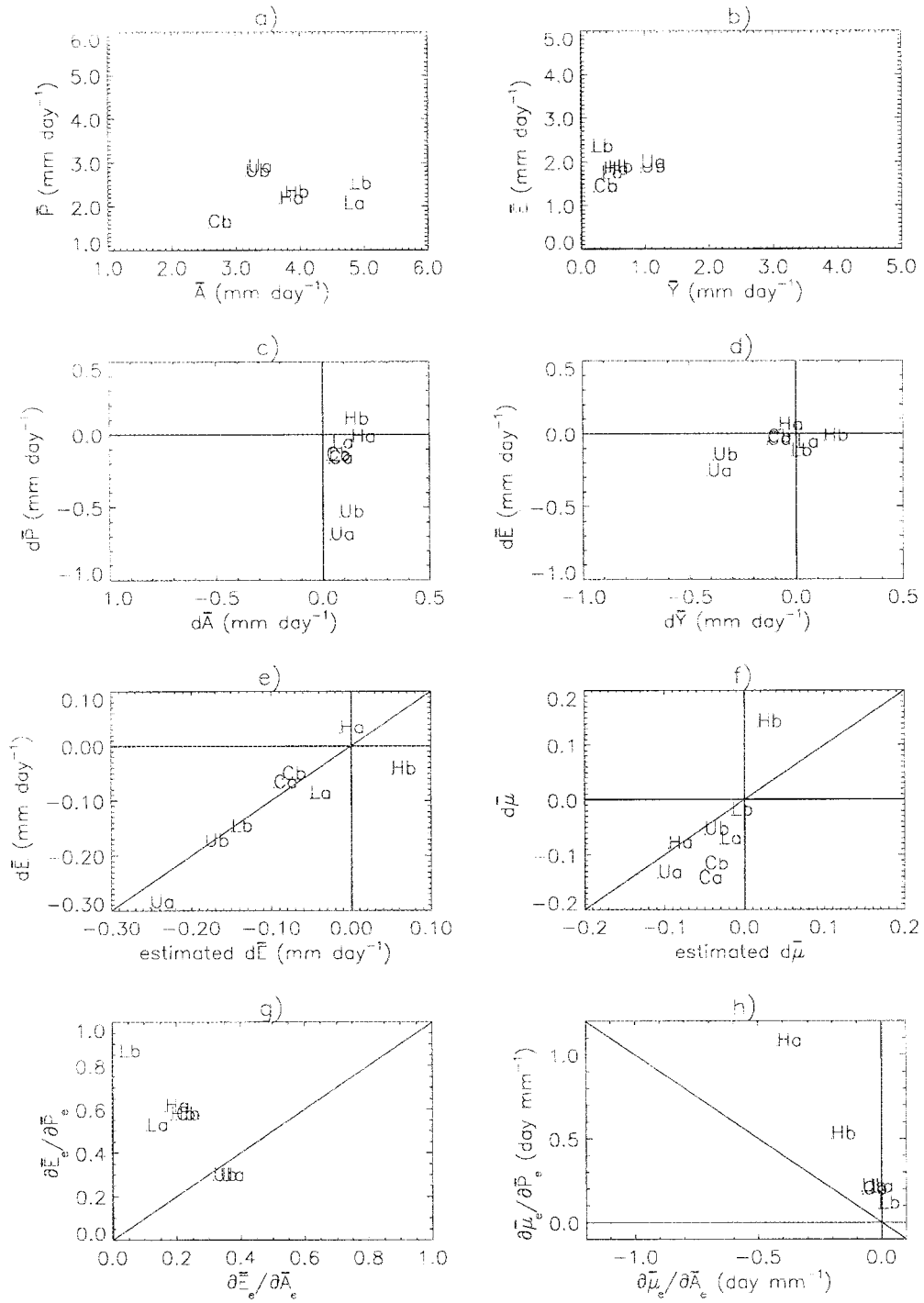

FIG. 5. As for Fig. 4 but for the Sahel. [The observed annual mean precipitation from New et al. (1999) is 1.4 mm day^{-1}.]

cessfully reproduces the predicted changes in evaporation and soil moisture for those models that do not include CO_2-induced stomatal closure (i.e., all but Hb and Cb, see Figs. 4e and 4f). The LSS responses vary from being almost completely dominated by energy availability to being mainly dependent on throughfall supply (see Fig. 4g), as a result of their very different hydrological states under the $1 \times CO_2$ climate. The Ha and Ca models are not moisture stressed in the control climate (see Fig. 2b and section 3a), which makes them insensitive to precipitation changes but very sensitive to changes in available energy (see section 3b). By con-

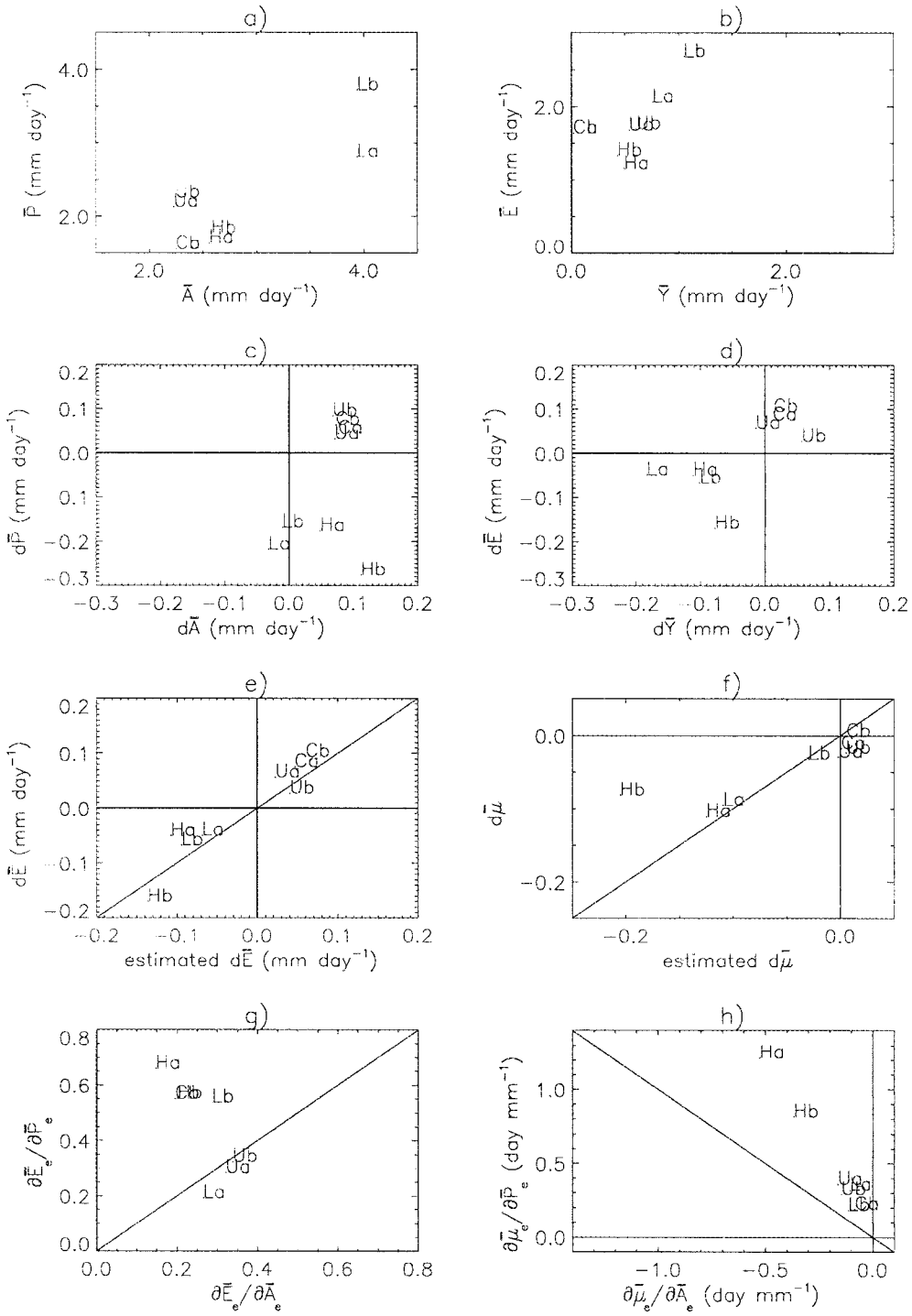

FIG. 6. As for Fig. 4 but for southern Europe. [The observed annual mean precipitation from New et al. (1999) is 2.4 mm day^{-1}.]

trast, the ''U'' and ''L'' models are moisture stressed in the control state and thus more responsive to the precipitation decrease than the available energy increase.

The characterization does not reproduce the hydrological changes for Hb and Cb, because CO_2-induced stomatal closure in these models tends to conserve soil moisture by reducing the values of f_c and f' in the 2 $\times$ CO_2 simulations (while the perturbation analysis of section 3b implicitly assumes that these characteristics are unchanged). However, the difference between the

GCM changes and those estimated using the linear characterization, as shown in Figs. 4e and 4f, does provide an indication of the direct impact of stomatal closure in these models. On this basis, Hb produces a markedly smaller reduction in soil moisture and a markedly greater reduction in evaporation than would be expected in the absence of this effect. The impact is much smaller in Cb, despite the fact that it was subject to similar changes in the stomatal conductance of the vegetated area (Douville et al. 2000). This is probably because transpiration makes up less of the total evaporation in this model. As a result of such differences, the impact of a physiological forcing (such as stomatal closure) is also likely to be very dependent on the host LSS.

Last, note the very different changes in precipitation and evaporation as predicted by the Ua and Ub models. These differ only in the prescribed plant rooting depth (see Table 1), which determines the size of the available soil moisture store, the seasonality of evaporation, and thus potentially the atmospheric water cycle. It is evident that this change has little impact on the control state, but has a major effect on the climate change and the hydrological response to this change (see Ua and Ub in Figs. 4c and 4d). This is therefore a further example showing that the impact of a LSS change on the simulation of the $1 \times CO_2$ climate is not a good indicator of its likely impact on a climate change prediction.

b. The Sahel

In the Sahel, all the models except Ca and Cb significantly overestimate the annual mean precipitation, and there is a large spread among the simulated values of annual mean available energy (Fig. 5a). As in Amazonia, the control states tend to be paired by GCM, with the possible exception of the LMD models. All the models apart from Hb show a reduction in annual mean precipitation, and an increase in available energy on doubling CO_2. The linear characterization reproduces the changes in evaporation and soil moisture effectively (Figs. 5e and 5f), and so it can be legitimately used to analyze the main differences in model behavior.

There is a significant scatter in the LSS sensitivities, which vary from being almost entirely throughfall dependent (Lb) to being sensitive to both forcing parameters (Ua and Ub) (see Fig. 5g). All the models are in similar hydrological regimes in the control state with $\overline{\mu} \leq 1$, so their different sensitivities must be a result of different values of ϕ and χ (see section 3b). For example, Ua and Ub have a similar aridity index (ϕ) to Ha and Hb, but substantially higher χ values as a result of their very different runoff curves (see Fig. 1f). This results in the ''U'' models having a much lower sensitivity to throughfall (see section 3b). The Lb and La models have quite different sensitivities to each other, but variations in ϕ are the primary reason for this. The bucket model (Lb) has no surface resistance, which results in a larger value of the maximum evaporative fraction (f_c), a larger value of ϕ [see Eq. (12)], and a greater sensitivity to throughfall.

c. Southern Europe

There is a large disparity in the GCM control climates for southern Europe (Fig. 6a), with the LMD models strongly overestimating precipitation and simulating much more available energy than the other models. The University of Reading models simulate rainfall close to observations, whereas the Hadley Centre and CNRM models underestimate it. Generally, there is also a large scatter in the simulated evaporation (Fig. 6b). All but the LMD models show an increase in available energy on doubling CO_2, but there is no consensus even on the predicted sign of the annual mean change in rainfall (Fig. 6c). The Hadley Centre and LMD models simulate a reduction in precipitation and evaporation, while the CNRM and University of Reading models predict increases in both variables.

Once again, the linear characterization appears to be capable of reproducing the changes in soil moisture and evaporation, for all the models except Hb (where CO_2-induced stomatal closure has a significant impact). The aridity index (ϕ) is relatively high, which ensures that each model is moisture stressed for at least part of the year. As in the Sahel, the models with lower critical runoff values (and thus lower values of χ) are most sensitive to changes in throughfall, while the different sensitivities of the ''L'' models are primarily due to the absence of a surface resistance in Lb.

d. Summary

Here we summarize some general findings from the regional analyses above.

- For most models the linear characterization effectively reproduces the changes in evaporation and soil moisture on doubling CO_2.
- The climate change anomalies appear to be much more dependent on the LSS than are the control climates, because of the differing LSS sensitivities to changes in precipitation and available energy.
- These varying sensitivities may arise from differences in the ''aridity'' of the control climate (ϕ) or from differences in the runoff fraction at the critical point (χ). The largest ranges in the sensitivity coefficients are typically associated with models that experience different hydrological regimes in the control state.
- The absence of an additional surface resistance to evaporation in the standard bucket model (Lb), significantly affects the control state and its sensitivity (primarily through its impact on ϕ).
- Otherwise, the runoff at the critical soil moisture (Y_c) seems to be the key LSS characteristic, since it controls the value of χ, and therefore the hydrological regime (see section 3a) and its sensitivity to climate change.

- The impact of CO_2-induced stomatal closure can be estimated from this methodology, and generally results in reduced evaporation, with a magnitude that appears to be very model dependent.

5. Discussion

We have analyzed results from eight climate change experiments, carried out with four separate GCMs, each of which used two distinct land surface schemes (LSSs). In the absence of a common coupling interface, such as that currently under development in PILPS phase 4 (Polcher et al. 1998), it was not feasible to use the same LSS in more than one GCM. Instead, the differences between the LSSs were chosen at the discretion of each participating group. This approach prevented the complete diagnosis of the impact of each LSS (including feedbacks), but guaranteed that a large range of parameterizations would be used.

To understand the role of the LSSs in the GCM simulations of climate and climate change, a simple characterization has been developed based on a generic ''bucket'' model, in which each LSS is described by curves representing runoff (Y) and evaporative fraction (f) as a function of scaled rootzone soil moisture (μ). This characterization has been applied to isolate the impact of LSS differences on the GCM-predicted changes in surface hydrology, over three very different climatic regions (Amazonia, the Sahel, and southern Europe).

A linearization of the bucket model was able to reproduce the very different soil moisture regimes experienced by each GCM–LSS pair. In each region, the range of simulated soil moistures was shown to be dependent on the variation between both the LSSs and the control climates. There is also likely to be a feedback between the two from moisture recycling. There are considerable deficiencies in some of the simulated control climates and hydrology. For example, some models simulated low precipitation and high moisture stress over Amazonia, while others produced marginal stress in the Sahel. The most important LSS differences were summarized in terms of the runoff, Y_c, which occurs when evaporation is marginally moisture-limited (i.e., at the critical soil moisture). The higher this critical point runoff is, the more moisture stressed the model tends to be.

Our analysis suggests that the relationship between climate and evaporation sensitivity is actually highly dependent on the characteristics of the LSS. Recently, Koster and Suarez (1999) have shown that the sensitivity of evaporation rate to climate variability can be understood in terms of a local aridity index. They have also shown this to be the case for the Amazonian simulations presented here (R. Koster and M. Suarez 1999, personal communication). The success of these two different methodologies, suggests that the atmosphere and land are closely coupled, with not only the atmosphere influencing the surface state, but also the LSS altering the atmospheric state. For example, over Amazonia the LSSs that had a tendency to be stressed, produced low evaporation that correlated with unrealistically low rainfall.

The variation in the LSS responses has been analyzed by partitioning the behavior into two parts; throughfall and available energy sensitivity. In very arid regions, evaporation is primarily dependent on throughfall changes, but this sensitivity decreases significantly with increased critical runoff. In moist climates, the models may range from being mainly sensitive to available energy changes, if they are unstressed, to being predominantly sensitive to throughfall, if moisture stressed.

Such a large spread was simulated over Amazonia. This explained why only four out of the six LSSs without CO_2-induced stomatal closure simulated a reduction in evaporation, even though they all had qualitatively similar forcing perturbations. The models singled out here tended not to be moisture limited and were therefore more dependent on the available energy increase than the rainfall reduction. Such gross variation in the land surface response can occur in any region that experiences perturbations in precipitation and available energy that are of opposite sign. In the other regions studied there was also a substantial scatter in the LSS sensitivities.

In some respects, the use of regional averages complicates the analysis, because the nonlinear nature of the evaporative fraction and runoff curves makes them sensitive to soil moisture heterogeneity. However, the idealized, piecewise linear f–μ curve still appears to offer a valuable conceptual model, separating the moisture-limited and non-moisture-limited regimes clearly. Also, while soil moisture heterogeneity might be expected to enhance regional-scale runoff, differences among the LSS runoff characteristics were much larger than could be explained by different subregional soil moisture distributions (not shown). Instead, the different LSS runoff characteristics are probably indicative of assuming different parameters at the gridpoint scale.

For example, the LSS used in the Hadley Centre ''b'' experiment shares a similar soil model structure to that used in the University of Reading simulations. Both LSSs use Darcy's equation to simulate vertical flow between four soil layers and each describes the variation of soil water suction and hydraulic conductivity with soil moisture concentration according to Clapp and Hornberger (1978). Both schemes also have similar definitions of the wilting and critical soil moisture concentrations (defined as the soil moistures for which the suction equals -1.5 MPa and -0.0033 MPa, respectively). The major differences are in the choice of extremely variable soil parameters such as the saturated soil water suction and the saturated hydraulic conductivity. The different values chosen yield values of Y_c of 1.3 and 0.014 mm day^{-1} for Ua (Ub) and Hb, respectively, in Amazonia. Such a discrepancy partially ex-

plains the very different moisture regimes simulated in these experiments.

Overall, our analysis supports many of the conclusions of Koster and Milly (1997). We have found that differences among the GCM predictions of changes in surface hydrology are particularly sensitive to how the runoff is parameterized over the active soil moisture range. Variations in the runoff at the critical soil moisture point (below which evaporation is moisture limited), account for much of the spread in the GCM predictions of hydrological change. Reducing the uncertainties in these predictions will require improved treatments of runoff appropriate for the GCM spatial resolution, rather than further sophistication in the treatment of evapotranspiration at the point scale.

Acknowledgments. This study was carried out as part of the EU Climate and Environment Programme under Contract ENV4-CT95-0112-PL950189. Peter Cox was also supported by the UK DETR Climate Prediction Programme under Contract PECD 7/12/37.

REFERENCES

Clapp, R., and G. Hornberger, 1978: Empirical equations for some soil hydraulic properties. *Water Resour. Res.,* **14,** 601–604.

Cox, P. M., R. A. Betts, C. B. Bunton, R. L. H. Essery, P. R. Rowntree, and J. Smith, 1999: The impact of new land surface physics on the GCM simulation of climate and climate sensitivity. *Climate Dyn.,* **15,** 183–203.

Douville, H., S. Planton, J.-F. Royer, D. B. Stevenson, S. Tyteca, L. Kergoat, S. Lafont, and R. A. Betts, 2000: Relevance of the vegetation feedbacks in double-CO_2 timeslice experiments. *J. Geophys. Res.,* in press.

Ducoudre, N., K. Laval, and A. Perrier, 1993: SECHIBA, a new set of parameterizations of the hydrologic exchanges at the land–atmosphere interface within the LMD atmospheric general circulation model. *J. Climate,* **6,** 248–273.

Entekhabi, D., and P. Eagleson, 1989: Land surface hydrology parameterization for atmospheric general circulation models including subgrid spatial variability. *J. Climate,* **2,** 816–831.

Gates, W., 1992: The Atmospheric Model Intercomparison Project. *Bull. Amer. Meteor. Soc.,* **73,** 1962–1970.

Gregory, J. M., J. F. B. Mitchell, and A. J. Brady, 1997: Summer drought in northern midlatitudes in a time-dependent CO_2 climate experiment. *J. Climate,* **10,** 662–686.

Henderson-Sellers, A., K. McGuffie, and A. Pitman, 1996: The Project for Intercomparison of Land-Surface Parametrization Schemes (PILPS): 1992–1995. *Climate Dyn.,* **12,** 849–859.

Houghton, J. T., L. G. M. Filho, B. A. Callander, N. Harris, A. Kattenberg, and K. M., Eds., 1996: *Climate Change 1995.* Cambridge University Press, 572 pp.

Koster, R. D., and P. C. D. Milly, 1997: The interplay between transpiration and runoff formulations in land surface schemes used with atmospheric models. *J. Climate,* **10,** 1578–1591.

——, and M. J. Suarez, 1999: A simple framework for examining the interannual variability of land surface moisture fluxes. *J. Climate,* **12,** 1911–1917.

Manabe, S., 1969: Climate and ocean circulation. 1. The atmospheric circulation and the hydrology of the earth's surface. *Mon. Wea. Rev.,* **97,** 739–774.

Mitchell, J. F. B., T. C. Johns, J. M. Gregory, and S. F. B. Tett, 1995: Climate response to increasing levels of greenhouse gases and sulphate aerosols. *Nature,* **376,** 501–504.

New, M., M. Hulme, and P. Jones, 1999: Representing twentieth-century space–time climate variability. Part 1: Development of a 1961–90 mean monthly terrestrial climatology. *J. Climate,* **12,** 829–856.

Noilhan, J., and S. Planton, 1989: A simple parameterization of the land surface processes for meteorological models. *Mon. Wea. Rev.,* **117,** 536–549.

Polcher, J., and Coauthors, 1998: A proposal for a general interface between land surface schemes and general circulation models. *Global Planet. Change,* **19,** 261–276.

Viterbo, P., and A. Beljaars, 1995: An improved land surface parameterization scheme in the ECMWF model and its validation. *J. Climate,* **8,** 2716–2748.

Warrilow, D. A., and E. Buckley, 1989: The impact of land surface processes on the moisture budget of a climate model. *Ann. Geophys.,* **7,** 439–450.